ACS APPLIED MATERIALS & INTERFACES

Research Article

www.acsami.org

Towards Tunable Sensitivity of Electrical Property to Strain for Conductive Polymer Composites Based on Thermoplastic Elastomer

Lin Lin, Siyao Liu, Qi Zhang, Xiaoyu Li, Mizhi Ji, Hua Deng,* and Qiang Fu*

College of Polymer Science and Engineering, State Key Laboratory of Polymer Materials Engineering, Sichuan University, Chengdu 610065, China

Supporting Information

ABSTRACT: The use of conductive polymer composites (CPCs) as strain sensors has been widely investigated and various resistivity-strain sensitivities are desirable for different applications. In this study, the use of mixed carbon fillers and functionalized carbon nanotubes was demonstrated to be vital for preparing thermoplastic polyurethane (TPU)-based strain sensors with tunable sensitivity. To understand the strain sensing behavior, we carried out scanning electron microscopy (SEM), Raman spectroscopy, wide-angle X-ray diffraction (WAXD), mechanical test, and rheology-electrical measurement. Hybrid fillers of multi-walled carbon nanotubes (MWNTs) and carbon black (CB) could reduce the entanglement in conductive network structure, thus increase the resistivity-strain sensitivity. Furthermore, incorporation of additional functionalized MWNTs in the CPCs could enhance the interfacial interaction between nanofillers and TPU, leading to further increase in sensitivity. Through such a simple method, strain sensors could be efficiently fabricated with large strain-sensing capability (strain as large as 200%) and a wide range of strain sensitivity (gauge factor ranging from 5 to 140238). Finally, the exponential revolution of resistive response to strain was fitted with a model based on tunneling theory by Simmons. It was observed that the change in tunneling distance and the number of conductive pathways could be accelerated significantly by adjusting conductive network structure and interfacial interaction. This study provides a guideline for the preparation of high-performance CPC strain sensors with a large range of resistivity-strain sensitivity.

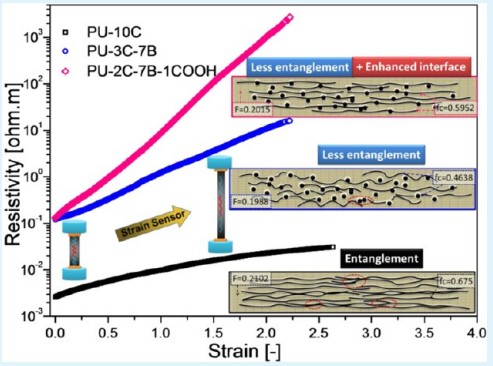

KEYWORDS: *strain sensor, conductive polymer composite, sensitivity, interfacial interaction, network structure*

1. INTRODUCTION

Conductive polymer composites (CPCs) have attracted increasing amounts of attention because of their wide range of application and easy fabrication methods.[1−3] Carbon nanotubes (CNTs) have been considered as one of the most suitable conductive fillers for the preparation of CPCs because of their large aspect ratio and ultra-high conductivity.[4] Recently, CPCs have been proposed to act as sensors for various stimulis, such as: strain,[5] damage,[6] stress,[7] temperature,[8] light,[9] and vapor.[10,11] In terms of strain sensing, a wide range of applications have been demonstrated, including: smart textile,[12−14] health monitoring,[15] wearable electronics,[16] movement sensor,[17] etc.

Different strain sensitivities, which can be expressed as gauge factor, are often required for different applications. Therefore, the control of sensitivity for strain sensors is considered as one of the most important issues.[5,18,19] To modify the strain sensitivity of CPCs, several methods have been demonstrated.[20−23] Hwang et al.[23] reported that the sensitivity of poly(dimethylsiloxane) (PDMS)-MWNT composites is strongly depended on the content of poly(3-hexylthiophene) (P3HT) wrapped around CNT bundles. And Dang et al.[22] observed that CNT with higher aspect ratio is preferred for higher sensitivity in CNT/silicone rubber nanocomposites. Murugaraj et al.[21] observed that narrow distribution of tunnel gaps between overlapping nanochannels is responsible for the high electromechanical sensitivity of their CPCs. In our recent work, it was demonstrated that mixed fillers containing CNT and metallic particle in different volume ratios can be used to modify the strain sensitivity of CPCs fibres.[24]

In the above investigations, various issues have been considered for the control of strain sensitivity in CPCs. However, the range of tunable strain sensitivity is still quite small. A systematic and efficient method is still needed for the control of sensitivity. A fundamental aspect of strain-sensing CPCs needs to be re-considered for the preparation of high performance strain sensor with tunable strain sensitivity. The electrical conductivity in CPCs is entirely provided by their conductive networks formed with conductive filler.[25] Therefore, the morphology of conductive network might play a crucial role on the strain sensitivity. Conductive networks formed with mixed carbon fillers have been extensively investigated[26,27] and it was concluded that different conductive network morphology

Received: April 17, 2013
Accepted: May 28, 2013
Published: May 28, 2013

could be constructed. However, the strain-sensing capability of these networks still needs to be investigated.

Furthermore, the change of conductivity under strain originates from the deformation of conductive network, particularly, the change of local contacts or tunneling distance between conductive fillers[28−30] and the orientation of conductive fillers.[31,32] To achieve these changes in CPCs, stress needs to be transferred from polymer to conductive fillers. It is reported that strong interfacial adhesion between functionalized MWNTs and thermoplastic polyurethane (TPU) matrix contribute to the overall mechanical properties of TPU/MWNT composites without sacrificing the elongation at break.[33] Likewise, the efficiency of stress transfer should play an important role on conductive network variation[15,34] and strain sensitivity.[35] Nevertheless, to the best of our knowledge, such an issue has yet to be investigated for strain-sensing CPCs despite of its vital importance.

Herein, CPCs based on TPU and hybrid carbon nanofillers in different dimensions will be fabricated. TPU is selected as matrix because of its wide range of applications, large elongation at break, and good affinity with carbon fillers.[30,32] The effect of conductive network morphology and interfacial interaction on the strain-sensing capability of these CPCs will be investigated. Because of the difference in filler dimension and intrinsic structure, the networks formed with mixed fillers might illustrate interesting strain-sensing behavior in CPCs. Furthermore, additional functionalized MWNTs (MWNT-COOH) were added to enhance interfacial interaction, thus optimizing the resistivity-strain sensitivity and obtaining high-performance strain sensors with tunable sensitivities.

2. EXPERIMENTAL SECTION

2.1. Materials. MWNTs produced by Nanocyl S.A. (Belgium), under the trade name of NC 7000, were used as conductive filler in CPCs. These MWNTs have an average diameter of 10 nm, length of 1.5 μm and a specific surface area of 250-300 $m^2\ g^{-1}$ according to the producer. CB (VXC-605, Cabot Co. Ltd, U.S.) is acetylene carbon black with DBP adsorption of 148 cm^3/100 g, and a primary particle diameter of 34 nm. Carboxylic acid functionalized MWNTs (−COOH content of 3.86 wt %, average diameter of 4 nm, length of 20 μm and purity higher than 95% according to the producer) were purchased from Chengdu Organic Chemicals Co. Ltd., Chinese Academy of Sciences. Ionic liquids (ILs, 1-butyl-3-methylimidazolium bis[(trifluoromethyl)sulfonyl]imide) were purchased from Cheng Jie Chemical Co. (Shanghai). Polyester based thermoplastic polyurethane (TPU, Irogran PS 455-203) produced by Huntsman Corp. was used as matrix in the composites. According to literature,[36] this type of TPU consists of 9.9% 4,4′-methylenediphenylene isocyanate (MDI), 58.2% butyl diol, and 31.8% adipate segments with hydroxyl group or carboxyl group.

2.2. Sample Preparation. The stretchable conductive nanocomposites were fabricated with MWNTs, ILs and as-received TPU. MWNTs (0.1g) were mixed with ILs (1g) and subjected to grinding in an agate mortar for 1 h, giving rise to a "bucky gel" state and enhancing the interface between MWNTs and TPU. The pre-treated MWNTs were dispersed into tetrahydrofuran (50 mL) with a laboratory emulsion machine (WX500CY, Shanghai Weiyu Company). Then, the dispersed MWNTs were added into TPU (0.9 g) solution with tetrahydrofuran (50 mL) as solvent. The mixture was stirred at 40 °C for 10 h and sonicated for another 1 h. The resulting swollen gel was poured onto a polytetrafluoroethylene plate and dried at 80 °C for 2 h. ILs were subsequently recovered with Solxhlet extraction (ethanol as the solvent) and the resulting composites were dried in the oven again at 80 °C for 4 h. Composites with other carbon fillers (CB, or carboxylic acid functionalized MWNT) were fabricated in the same fashion.

In this paper, samples were denoted as PU-xC-yB-zCOOH, where *x*, *y*, *z* represents the weight fraction of MWNT, CB, and MWNT-COOH in TPU composites, respectively.

2.3. Characterization. *Tensile measurement and strain-sensing test.* Composite films were clamped between a pair of aluminum electrodes, creating a gage length of 50 mm. Resistance was measured with a Keithley 6487 picoammeter under a constant voltage of 1 V to avoid strong electric current within the sample. Resistivity exceeding 1×10^6 Ohm m is not measurable with current set-up and these samples are therefore classified as non-conductive. Silver paint was applied to both ends of the sample to ensure good contact. The samples were stretched in a SANS CMT4000 universal testing machine. The resistance measurement set up and tensile test machine are both interfaced with a computer as illustrated in Figure S1 in the Supporting Information to record the resistivity-strain dependence of these CPCs. A constant rate of 5 mm/min was used for the resistance-strain measurement. Cyclic stretching and recovery was also conducted to investigate the dynamic resistance-strain behavior. The program of cyclic deformation includes stretching to 100% strain (100 mm) at 5 mm/min, pausing for 2 s, and withdrawing at 5 mm/min to the initial length of 50 mm.

Rheology-electrical measurement. Rheological measurement was performed on an advanced rheomitric expansion system (ARES, Rheometrics Co., USA) in dynamic time sweep mode under 3% strain amplitude with an angular frequency of 0.628 rad/s. Simultaneously, R was measured at a direct current voltage 1 V with an automatic measurement system where a 7150 plus digital multimeter (Schlumberger) was installed. Dynamic frequency sweep to TPU was conducted from 0.01 to 100 rad/s in the linearity region. The sample was prepared by thermal compressing into a round plate with thickness of 25 mm diameter and 3 mm thickness.

Scanning electron microscopy. Morphological studies were carried out using a SEM (JEOL JSM-5900LV) under an accelerating voltage of 20 KV. To investigate the conductive networks below sample surface, un-coated specimens were used. The conductive networks in the polymer matrix are charged to emit enriched secondary electrons to make them visible.[37]

Raman spectra. Raman spectra were recorded on a micro-Raman spectrometer (JY HR800) equipped with a microscope. Excitation was provided by He−Ne at 786 nm. A beam size of 1 μm was used. For polarized Raman spectra, the film was rotated 90° so that the E-vector of polarized laser light was parallel and perpendicular oriented to the drawing direction. All spectra were baseline corrected and the peak position and intensity were fitted in range from 1000 to 2000 cm^{-1}.

2D-WAXD. Two-dimensional wide-angle X-ray diffraction (2D-WAXD) measurements were conducted on a Bruker DISCOVER D8 diffractometer. XRD data were collected for each point on the library sample at ambient temperature using Cu−Kα radiation for 100 seconds. The film samples were placed with the beam perpendicular to the drawing direction. The background of all 2D-WAXD patterns given in this article had been extracted and thus allows a qualitative comparison

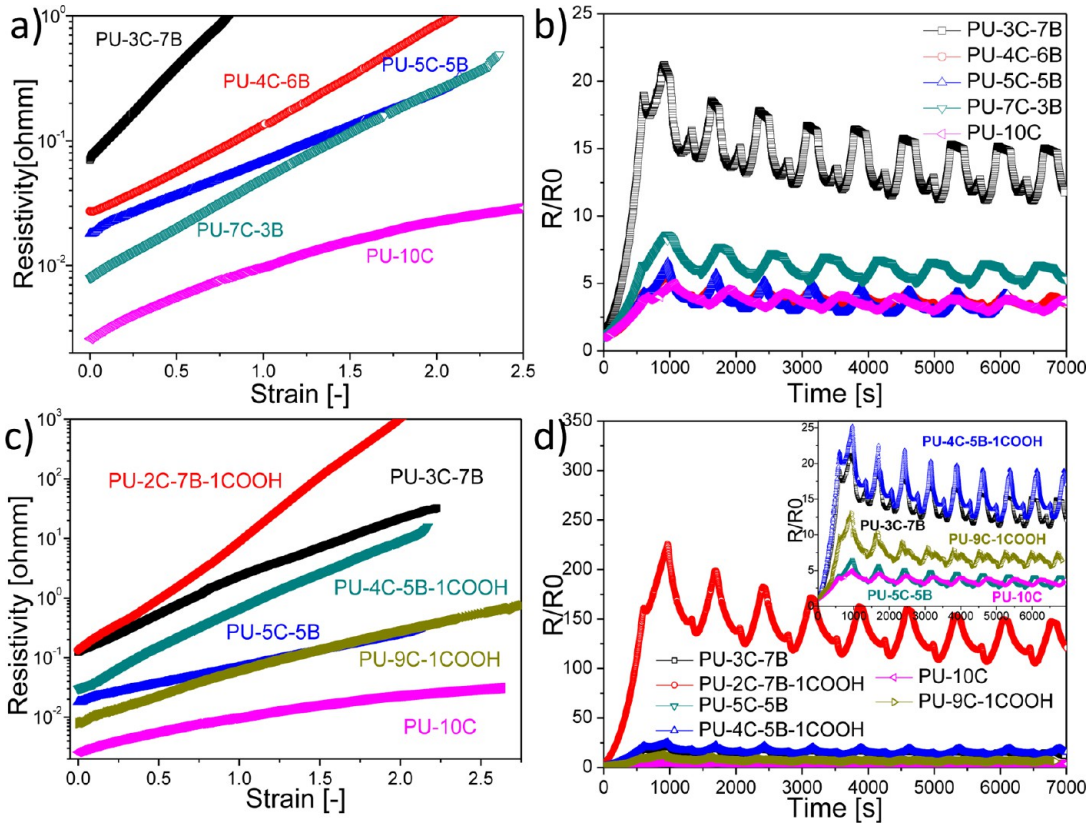

Figure 1. Strain-sensing behavior measurement for TPU/MWNTs/CB composites: (a, c) Resistivity-strain (b, d) relative R-time relationship.

between various samples. X-ray data were recorded in the scattering from 0 to 35°.

3. RESULTS AND DISCUSSION

3.1. Strain-Sensing Behavior of CPC. Because the electrical properties of CPCs are entirely provided by their embedded conductive networks, the structure of conductive network should play an important role on the strain-sensing behavior of these CPCs. To investigate its effect, CB particles are added into CPCs containing MWNTs. As shown in Figure 1, a total content of 10 wt % carbon nanofillers was used. It has been reported that entangled single-walled carbon nanotubes (SWNT) or MWNT bundles can be exfoliated into much finer bundles and a gel-like material can be formed by grinding them with imidazolium-based ionic liquid (IL).[32,38] Therefore, MWNTs were firstly treated with IL before mixing with TPU to enhance the dispersion of MWNTs. The linkage between IL-MWNTs and TPU polymer chains by physical or chemical bonds enhance the uniform dispersion of MWNTs in TPU matrix, since it is noted that the composites without IL is not able to withstand high strain. As shown in Figure 1a, the electrical conductivity of composites containing 10 wt % MWNTs reaches 384.6 S/m (resistivity 0.0026 Ohm m). The resistivity of all CPCs increases gradually with increasing strain, which agrees with previous reports.[24,30] It is noted that all TPU/MWNT/CB samples can be elongated to more than 250% strain before rupture. Hence, it is considered that uniform dispersion of carbon fillers in TPU has been achieved. Morphological observations using SEM also confirm that relatively uniform dispersion has been achieved (see Figure 3).

Figure 1a shows the resistivity changes of TPU/MWNT/CB composites under uniaxial strain. As indicated by the slope coefficient of resistivity−strain ($\rho-s$) curve, higher CB proportion in carbon fillers contributes to higher resistivity and higher $\rho-s$ sensitivity. The large aspect ratio of MWNTs is often reported to be beneficial for the formation of conductive network and overlapping between MWNTs compared with CB particles of low aspect ratio.[39] Thus, less entangled networks are formed with hybrid fillers. This directly leads to higher sensitivity at the same filler concentration for hybrid fillers. Among all these CPCs in Figure 1a, PU-3C-7B composite demonstrates the highest $\rho-s$ sensitivity and an initial conductivity of 14.2 S/m.

This can be further verified by dynamic strain-sensing behavior shown in Figure 1b. As the application of strain sensing often requires reversible strain loadings, CPCs were subjected to cyclic strain profiles. The relative resistance (R/R_0) is plotted from zero-strain against time. It is noted that the resistivity generally increases with increasing strain, and decreases with decreasing strain. This can be defined as positive strain effect.[40] In addition, shoulder peaks are observed during these cycles, which might originate from the competition between destruction and reconstruction of conducting pathways during dynamic loadings.[6,41,42] To further explore the reversibility, the stretchable conductive nanocomposite film was strained 100% and relaxed to its unstrained state cyclically for 36 times. Figure S3a in the Supporting Information shows R/R_0 as a function of time marked with the number of uniaxial stretching/releasing cycles. A gradual decrease in resistivity peak is observed in the first 8 dynamic cycles, which is thought to be caused by the formation of additional conductive pathways through the breakdown of interface between polymer and filler.[29] However, during cycles 9−36, the drifting is much less obvious and almost stabilized.

dx.doi.org/10.1021/am401402x | ACS Appl. Mater. Interfaces 2013, 5, 5815−5824

Therefore, the strectchable nanocomposite shows a high level of strain (100%) without a notable degradation of conductivity after many stretching/relaxing cycles. The resistivity becomes recoverable and the strain sensing behavior remains stable after 8 stretching/releasing cycles.

As discussed in the Introduction, the interfacial interaction between filler and matrix might play an important role on the strain-sensing behavior of CPCs. To investigate this issue, we replaced some of the raw MWNTs with MWNT-COOH. It is observed from Figure 1c that the initial resistivity slightly increases due to defects on MWNT-COOH brought in during the functionalization process. More importantly, the $\rho \sim s$ slope rises after incorporating MWNT-COOH into composites, indicating enhanced strain sensitivity. For CPCs containing a total filler content of 10 wt % (see Figure 1c), it is noted that the network structure (using mixed fillers by replacing 7 wt % MWNTs with 7 wt % CB) and interfacial interaction (using 1 wt % functioned MWNTs replacing 1 wt % pristine MWNTs) can be both used to modify the strain-sensing behavior of these CPCs. More importantly, these two effects can be combined to further enhance the strain sensitivity of these CPCs. As a result, the resistivity of PU-2C-7B-1COOH increases by 4 orders of magnitude, whereas that of PU-10C only increases by 1 order of magnitude under 200% strain. As shown in Figure 1d, dynamic strain-sensing behavior is also conducted to investigate the strain sensitivity and enhanced sensitivity is obtained as shown in PU-2C-7B-1COOH. Regarding the nature of such enhanced interfacial interaction, the hydroxyl groups on TPU matrix and carboxyl groups on MWNT-COOH are expected to form relatively strong interaction, hydrogen bond. This phenomena is often observed between functionalized CNT and polymer with active polar groups.[33,43−45]

On the other hand, interfacial interactions might be tuned by changing the functionalization degree or modifying the nature of active groups, such as amino-group. Herein, MWNT-COOH is selected because of its good interaction with polyester-based TPU. As shown in the literature,[46−48] high functionalization degree leads to worse electrical property, thus hindering the formation of efficient conductive network. Thus, we used functionalized MWNTs with 3.86 wt % carboxyl groups (−COOH) to keep a certain degree of functionalization as well as electrical conductivity. Indeed, a balance could be obtained with further study to achieve maximum strain sensitivity by tunneling the inter-play between degree of functionalization and electrical conductivity.

As well known, gauge factor (GF) can be introduced to quantify sensitivity for strain sensors.[20,49] GF is the instant ratio of relative change in electrical resistance to the mechanical strain.

$$\mathrm{GF} = \mathrm{d}(R/R_0)/\mathrm{d}s \quad (1)$$

R and R_0 refer to the resistance and initial resistance, whereas s represents strain. To achieve high sensitivity (a large change in resistance under the same strain), a higher value of GF is desirable. Conventional strain sensors, relying on geometrical change of conduction path, have GF in the range of 2−5 and represent a reliable and well-established technology. Other strain gauge types, such as silicon, exploit the piezoelectric character of the material and offer GF larger than 100. This type of sensor, however, is more fragile and often used for small strain. Kumar et al.[50] suggested the behavior of decreasing sensitivity with increasing nanotube content and GF of 1.49 to 3.28 can be achieved through the loss of contact between nanotubes in the matrix and enlarged tunneling resistance. The GF of pure MWNT network was experimentally determined at 0.34[51] or 7.[52] The calculated and measured GF of a sensor composed of multiple CNTs in a parallel resistor network was about 75[53] and aligned CNT film has a GF of 79−134.[54]

The GF of these TPU/MWNT/CB composites in current study can be calculated using data shown in panels a and c in Figure 1. The results are plotted to compare with some strain sensors reported in literature[20,21,52,54−58] (as shown in Figure 2a). It is observed that sample PU-2C-7B-1COOH is obviously

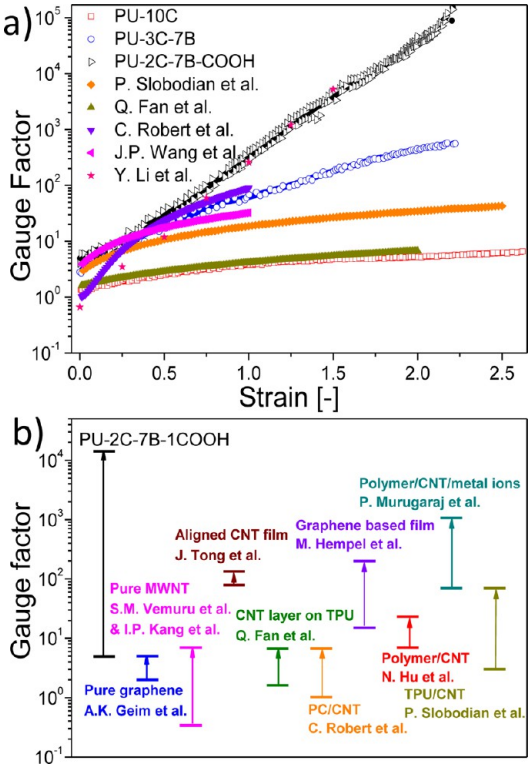

Figure 2. (a) Gauge factor as a function of strain; (b) range of sensitivity, compared with other papers[14a,14b, 30,31,33,34,36].

the most sensitive, with gauge factors around 5 at zero strain, and approximating 40000 at 200% strain and 140238 at 220% strain, which corresponds to drastic rise of resistivity with increasing strain. On the contrary, other samples have much smaller gauge factors as shown in Figure 2. Specifically, the GF of PU-10C increases linearly with strain from values around 1.35 at the beginning of deformation to nearly 5.5 at 200% strain, and PU-3C-7B has an initial factor of 2.76, which jumps to 443 at 200% strain. Besides, the GF during dynamic sensing process (100% strain magnitude) was plotted as a function of time in Figure S3b in the Supporting Information. It is observed that GF of PU-2C-7B-1COOH has the most drastic fluctuation, in accordance to the dynamic sensing behavior in Figure 1d. The exponential increase in resistance with applied tensile strain observed in CNT filled polymer composite systems, having GF < 50, has been identified as tunnel junction gap-width modulation between the overlapping CNTs.[59,60] Meanwhile, obtaining enhanced sensitivities (GF > 50) are often reported to be difficult in practice in these composites due to inhomogeneous mixing, irregular particle/CNT bundle sizes, wide distribution of tunnel gaps and presence of percolating.[58,61] As shown in Figure 2a, it is clearly

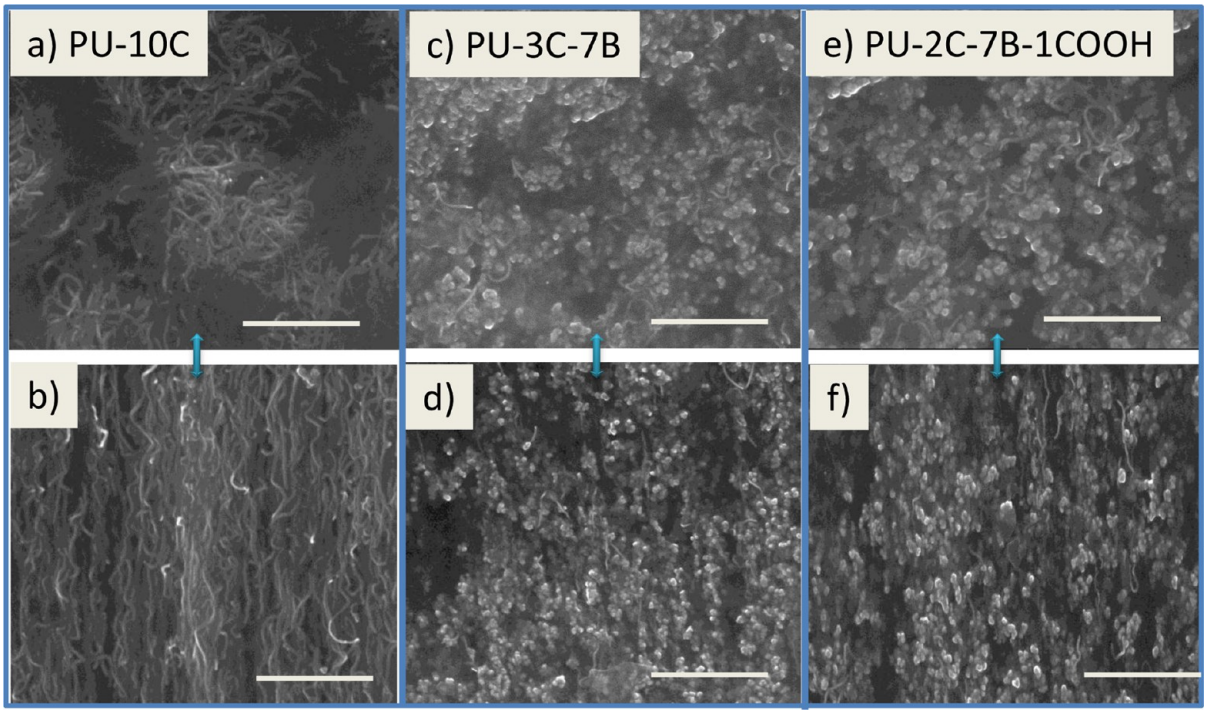

Figure 3. SEM morphological study of composites with different fillers: 10%MWNT-TPU composites, 3% CB-7%MWNT-TPU composites, 2%CB-7%MWNT-1%(f-MWNT-)TPU composites, from left to right; the downside SEM images (b, d, f) refer to the corresponding CPCs at 200% strain.

demonstrated that the effect of using hybrid fillers and enhanced interfacial interaction can be combined to further enhance the strain sensitivity of CPC strain sensors. As shown in Figure 2b, the range of tunable sensitivity is plotted to compare with some results reported in literature. It can be noted that a GF of 5 to 140238 (220% strain) is obtained in current study, which is much larger than the results reported previously.[20,21,51,52,54−56,58,61] Thus, strain sensors with a wide range of tunable GF can be fabricated through such a method combining tunable network structure and interfacial interaction. It can be used as a general guideline for the preparation of high-performance strain sensors with tunable sensitivity. To further understand the mechanism behind this, the following studies are carried out.

3.2. Microstructure of conductive networks and polymer matrix. *Morphology study.* To investigate the underlying mechanism of change in resistivity during stretching, we carried out morphological studies. The SEM images of conductive MWNT-CB networks in these CPCs were obtained under high accelerating voltage, causing conductive networks in the insulating matrix to become charged and emit enriched secondary electrons (see Figure 3). For Figure 3a, c, and e, the as-prepared CPCs of PU-3C-7B and PU-2C-7B-1COOH show an isotropic state. Because of their large aspect ratio and fibrous shape, MWNT-filled composites demonstrate entangled conductive networks. For CPCs containing both CB and MWNTs, less entangled networks are demonstrated because of the low aspect ratio of CB. It is noted that the conductive networks formed with mixed fillers (see Figure 3) demonstrate a complex nanostructure of multiple MWNTs bridging adjacent CB particles and MWNT bundles gathering around CB particles.[28] Although these CPCs are stretched to 200% strain (as shown in Figure 3b, d, and f), MWNT bundles are aligned in the drawing direction and CB particles are also stretched into oriented structure. The orientation of MWNTs is more pronounced than that of conductive network in PU-3C-7B. This might be caused by the more entangled network of MWNTs, as such a network can transfer the shear applied on the network more efficiently. Furthermore, it can be also noticed that the deformation of conductive network and filler orientation in PU-2C-7B-1COOH may be greater than those in PU-3C-7B.

Raman Spectroscopy. To confirm the morphology observed above, polarized Raman spectroscopy is used to study the orientation status of these MWNTs (see Figure 4a). Resonance-enhanced Raman scattering effect can be observed in MWNTs when a visible or near infrared laser is used as the excitation source and such a resonance effect is not observed for polymer matrix. Therefore, Raman spectroscopy is an ideal method to characterize the orientation status of CNTs. Two bands at around 1580 and 1350 cm^{-1} in the spectra are assigned to E_{2g} and A_{1g} modes, respectively. The former is denoted as the G-band generated by stretching mode of sp^2 atom pair in carbon ring or long chain and the latter is denoted as the D-band induced by structure disorder and flaw. Figure 4a shows significant changes in Raman absorption intensity of six samples within the region of 1000-2000 cm^{-1}. The D/D and G/G ratios parallel/perpendicular to the fiber axis increases for both bands in a similar manner and the intensity ratio of G band in both directions can be considered as an indicator of MWNT alignment in the composite films.

The dichroic ratio D[62]

$$D = A_{\parallel}/A_{\perp} \tag{2}$$

and the orientation function F

$$F = (D - 1)/(D + 2) \tag{3}$$

Here, $A_{\parallel}$ and $A_{\perp}$ are the absorption of a band measured with incident light polarized parallel and vertical to stretching

dx.doi.org/10.1021/am401402x | ACS Appl. Mater. Interfaces 2013, 5, 5815−5824

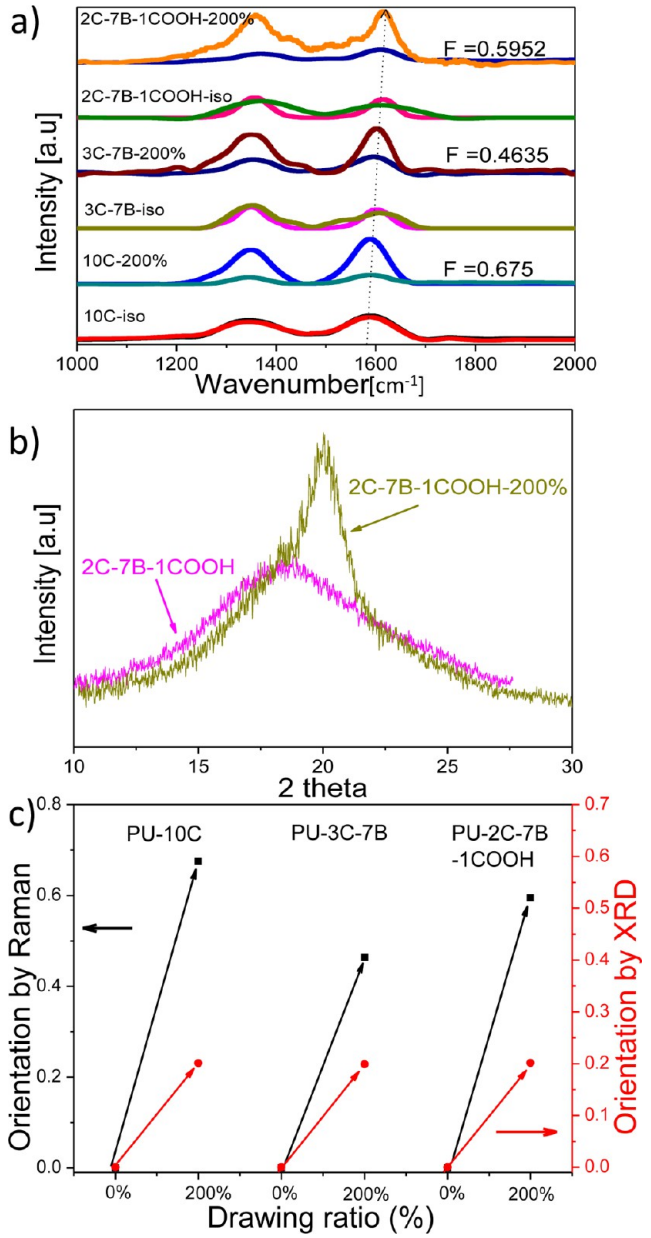

Figure 4. (a) Polarized Raman spectra and (b) 2D-WAXD data of TPU based nanocomposites, (c) contrast of orientation factors by Raman and 2D-WXAD.

direction, respectively. Higher alignment degree contributes to larger orientation function *F* value.

Under 200% strain, the PU-2C-7B-1COOH (F = 0.5952) exhibits a higher orientation factor than PU-3C-7B (F = 0.4638), whereas PU-10C composites possess the highest orientation factor of 0.675. This is in agreement with above strain-sensing behavior and morphological studies. By comparing PU-10C with PU-3C-7B under strain, the large overlap length between MWNTs and entangled dispersion status in PU-10C might be responsible for the higher orientation degree of MWNTs under strain. Thus, higher strain sensitivity is obtained for PU-3C-7B as the less entangled network is destructed more easily under strain than that of PU-10C. For two composites containing hybrid fillers (PU-3C-7B and PU-2C-7B-1COOH) under strain, a higher orientation is observed for MWNTs in PU-2C-7B-1COOH, as the improved interfacial interaction between conductive filler allows more efficient stress transfer. This leads to higher strain sensitivity observed above. This is also confirmed with mechanical properties shown in Figure S2, as higher tensile strength is observed for PU-2C-7B-1COOH.

Besides, it is also observed in Figure S4a in the Supporting Information that the peak of G-band shift to higher frequency after replacing 1 wt % MWNT with 1 wt % MWNT-COOH. This might be caused by the formation of strong interaction (or hydrogen bond)[33] between TPU matrix and functionalized MWNTs. Similar up-shifting of the G band has been reported for SWNT-reinforced epoxy resins[43,44] and polypropylene.[45] We may also ascribe the higher orientation of PU-2C-7B-1COOH (than that of PU-3C-7B) to the hydrogen bond and interfacial interaction. Therefore, PU-2C-7B-1COOH composites exhibit good respond to strain in both resistivity and orientation.

WAXD. Shear can often result in orientation in polymer matrix.[63−65] 2D-WAXD was also conducted to examine the structure of polymer matrix under strain for different composites. In the wide-angle region (Figure 4b), scattering peaks from the amorphous polymer (2θ = 17.6°, inter-planar spacing of 0.446 nm) and crystalline TPU soft-segments (2θ = 19.0°, inter-planar spacing of 0.413 nm) are visible. Note that the hard-segment crystalline does not seem to contribute to the X-ray pattern due to their low content and chemical structure.[36] And the graphene plane in the CNT sidewall ($2\theta \approx 25°$) is inconspicuous here. With increased elongation (from zero strain to 200% stain) the broad scattering maximum at 0.446 nm from the amorphous polymer gives way to a narrow reflection at 0.413 nm, indicating strain induced crystallization.[66]

The orientation level (Herman's factor, fc) can be obtained by the equations[31,67] below

$$\mathrm{fc} = \frac{3\langle \cos^2 \varphi \rangle - 1}{2} \tag{4}$$

$$\langle \cos^2 \varphi \rangle = \frac{\int_0^{\pi/2} I(\phi) \sin \phi \cos^2 \phi \, d\phi}{\int_0^{\pi/2} I(\phi) \sin \phi \, d\phi} \tag{5}$$

A characteristic feature of X-ray patterns from a uniaxial oriented sample is the presence of arcs. The azimuthal width of the arcs (see Figure S4c in the Supporting Information) provides information about the orientation degree of respective scattering planes.

Combining the WAXD data (see Figure S4b in the Supporting Information) with the above two equations, it can be obtained that the orientation degree increases with increasing strain, revealing fc values at 200% strain of 0.2102, 0.1988, 0.2015, for PU-10C, PU-3C-7B, and PU-2C-7B-1COOH, respectively. It is thought that TPU matrix in three different CPCs respond to 200% strain in similar fashion, showing similar orientation degree around 0.2.

Comparing the orientation changes of carbon fillers from Raman spectra with that of TPU from WAXD (Figure 4c), it is noted that the orientation of TPU matrix increases in similar fashion while conducting network exhibits different changes with addition of CB particles and functionalized MWNT. It should be mentioned that the orientation factor of TPU is relatively low as only 200% strain is applied. Nevertheless, it is interesting to observe that the orientation of conductive

network increases at different amplitudes for those three specimens. It is caused by the special network configuration described above, as the stress is transferred in different fashion from polymer matrix to conductive network. The difference in polymer matrix and filler orientation agrees well with the strain-sensing results observed above.

Rheological-Electrical Properties. Dynamic frequency tests were used to explore network formation and microstructure of the nanocomposites. The storage modulus (G') of neat TPU, TPU/MWNT, TPU/MWNT/CB nanocomposites measured at 150 °C is logarithmically plotted as a function of angular frequency (ω) in Figure 5a. The time−dependent relative resistance (R/R_0) for MWNT/CB/TPU composites is shown in Figure 5b.

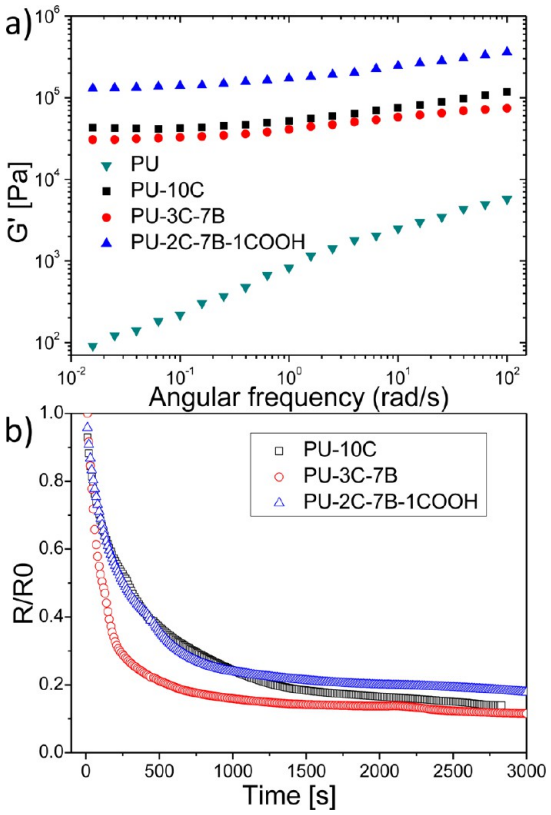

Figure 5. Logarithmical plots of (a) storage modulus vs. angular frequency; (b) time-dependent relative resistance at 150 °C and 0.628 rad/s.

Incorporation of carbon fillers into polymers causes dramatic changes in viscoelasticity of polymer melts, such as the modulus increment, the appearance of a low-frequency plateau for G', and so on. Besides, three types of network, i.e., a temporary filler network, a temporary polymer network formed by entanglement, and a combined filler−polymer network, have been proposed to explain the rheological behaviors of filled polymers.[68] Three types of carbon filler−polymer interactions[69] have been proposed to account for the agglomeration of MWNTs and CB aggregates: (a) direct bridging, (b) bridging through entanglement of adsorbed chains, and (c) bridging through entanglement of non-absorbed chains. These networks and interactions can result in a reduction in mobility of polymer molecules and thus lead to G' increment and plateau at low frequency, as shown in Figure 5a. The increment in G' of PU-2C-7B-1COOH mainly attributes to the enhanced adsorption between functionalized CNTs and TPU chains. Additionally, the slope of lgG' to lgω shifts from 0.461 (pure TPU) to 0.27 (TPU-10C), confirming the influence of MWNTs on viscosity of the composites. Besides, the magnitude of complex viscosity (η^*) of nanocomposites substantially increases with increasing filler loading because of the establishment of TPU-CNT and CNT−CNT interactions, which noticeably opposes the segmental chain molecular mobility of TPU matrix. As to the high content (10 wt %) of carbon fillers, there is obvious dependence of η^* on frequency without plateau at low frequency in Figure S5a in the Supporting Information.

The time-sweeps (150°C, 0.628 rad/s, 3% strain) in Figure 5b reveal the conductive network revolution during annealing. As discussed in our previous work,[31] the change of conductive network under annealing can reflect the network structure. The relaxation of polymer melt facilitated the diffusion and fluctuation of nanotubes, nano-spheres or their aggregates. For composites with CB, mobility of nanoparticles results in instant increase in G' and G' (or decrease in R/R_0) during early stage of melting annealing (see Figure S5b in the Supporting Information), whereas the large aspect ratio and entanglement of MWNTs hinder the electrical and mechanical variation. G' and G'' ascend with time as a consequent of conductive network recovery. For PU-2C-7B-1COOH, the rate of R/R_0 change is reduced because of enhanced interaction (see Figure 4b). Meanwhile, the enhanced interfacial interaction also lead to more enhancement in G' and G'' (see Figure S5b in the Supporting Information).

3.3. Modeling and Mechanism. To understand the strain-sensing mechanism, modeling study is carried out. According to the model[70] derived from tunneling theory by Simmons,[71] the total resistance R of the composites can be calculated using eqs 6 and 7

$$R = \left(\frac{L}{N}\right)\left(\frac{8\pi hs}{3\gamma a^2 e^2}\right)\exp[\gamma s] \tag{6}$$

$$\gamma = \frac{4\pi\sqrt{2m\varphi}}{h} \tag{7}$$

Where L is the number of particles forming a single conductive path, N the number of conducting paths, h the Plank's constant, s the least distance between conductive particles, a^2 the effective cross-section area, e the electron charge, m the electron mass, and φ the height of potential barrier between adjacent particles.

While strain is applied to the CPCs, the resistance will be altered because of particle separation and the interparticle distance changes linearly and proportionally with increased strain from s_0 to s. Then, it can be expressed as follows

$$s = s_0\left(1 + C\left(\frac{\Delta l}{l_0}\right)\right) \tag{8}$$

where ε is the tensile strain of the composites, Δl the deformation of the composite samples, and l_0 the initial length of the sample.

Because of the high rate of resistivity increase at larger strain, it is assumed that the number of conducting pathways changes at a much higher rate, and can be expressed as follows[72,73]

$$N = \frac{N_0}{\exp(M\varepsilon + W\varepsilon^2 + U\varepsilon^3 + V\varepsilon^4)} \tag{9}$$

where M, W, U, and V are constants.

dx.doi.org/10.1021/am401402x | ACS Appl. Mater. Interfaces 2013, 5, 5815−5824

The substitution of eqs 8 and 9 into eq 6 yields

$$R = B(1 + Cx)\exp[A + (2M + AC)x + 2Wx^2 + 2Ux^2 + 2Vx^2] \quad (10)$$

Where $x = \varepsilon$, $A = \gamma s$, $B = 8p\pi nhs_o/2\gamma N_o^2 a^2 e^2$.

It is shown in Figure 6 that the model of tunneling currents describes the experimental data quite well. Fitting parameters

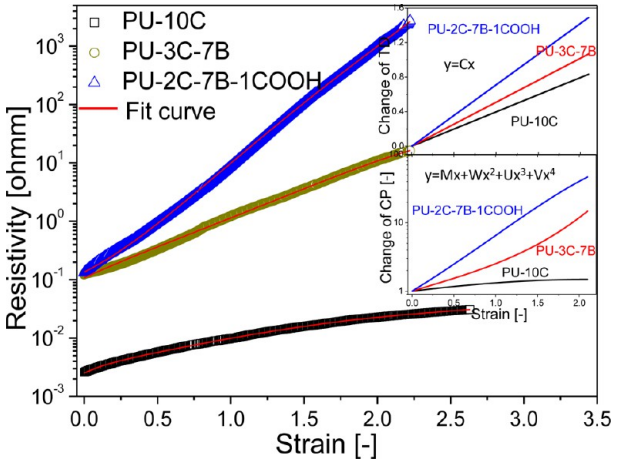

Figure 6. Experimental (dots) and theoretical (red solid lines) data of strain-dependent resistance for TPU composites. The inserted graph is the change of conducting pathway and tunneling distance and obtained parameters by fitting is listed in the Supporting Information.

are listed in Table S1 in the Supporting Information. The calculated change of conducting pathways (change of CP, $M\varepsilon + W\varepsilon^2 + U\varepsilon^3 + V\varepsilon^4$) and change of tunneling distance (change of TD, $C\varepsilon$) are plotted against strain as shown in the two insets in Figure 6. It is observed that the number of conducting path in PU-2C-7B-1COOH decreases much faster than that in PU-3C-7B, and PU-10C demonstrates the lowest change rate among all. Besides, the tunneling distance in PU-2C-7B-1COOH increases at higher rate than that in PU-3C-7B and PU-10C. Both aspects verify the fact that CPCs with MWNT-COOH have much better affinity to TPU matrix, and conductive network consisting of hybrid fillers is less entangled. These issues cause the conductive network to deform greatly under strain.

To gain a clear understanding of the network structure during strain sensing, a schematic representation is proposed in Figure 7. Isotropic conductive network often demonstrate significant increase in resistivity under strain due to strain induced orientation of conductive networks as shown in Figure 7. Such orientation could in turn result in loss in local contact between networks. The difference among these three CPCs, PU-10C, PU-3C-7B, and PU-2C-7B-1COOH, is the structure of conductive networks and varied interfacial interaction between the TPU matrix and carbon fillers under strain. This leads to quite different $\rho-s$ sensitivity. For PU-10C, MWNT bundles exhibit conspicuous orientation along the drawing direction at 200% strain. The entanglement between MWNT bundles and a large overlap length between them might be responsible for the network structure and electrical properties observed. On the other hand, CB particles fill in the gap between the ends of nanotube, but more often they aggregate between the MWNT bundles. It can be noticed that MWNT bundles seem curly along the alignment direction and CB particles lie on the bundles. Therefore, the CB particles in PU-3C-7B cannot act efficiently as the bridge of the enlarged tunneling distance between nanotubes under large strain, resulting in drastic conductivity drop under strain. More importantly, the improved interfacial interaction by using functionalized CNTs provides better load-transfer across polymer-MWNT matrix and larger driving force for the alignment of conductive network than that in PU-3C-7B. Therefore, the MWNT bundles are more oriented in PU-2C-

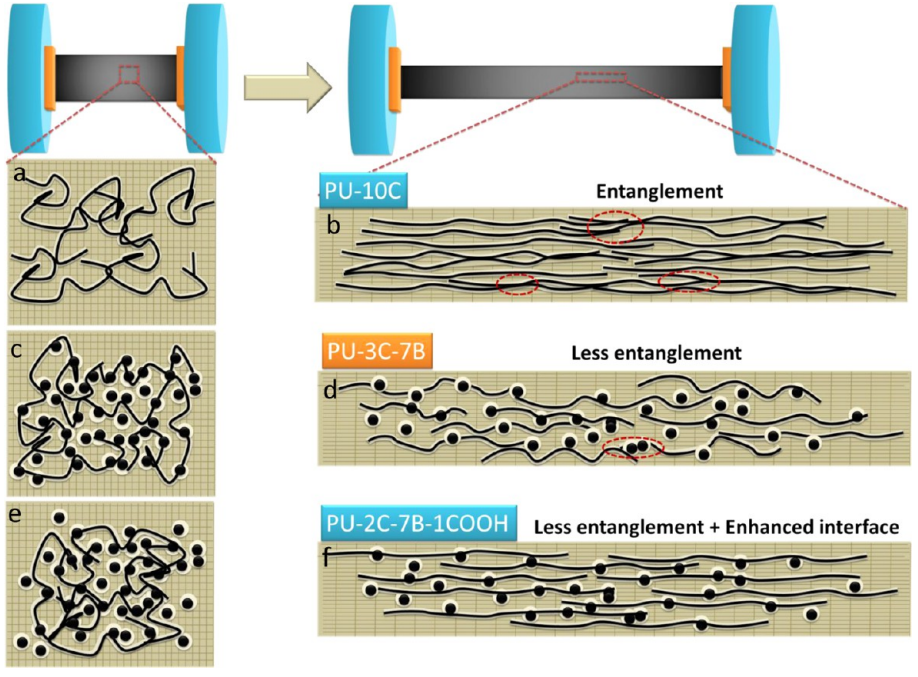

Figure 7. Sketch of MWNT network: (a) as-prepared PU-10C; (b) PU-10C sample at 200% strain; (c) as-prepared PU-3C-7B; (d) PU-3C-7B at 200% strain; (e) as-prepared PU-2C-7B-1COOH; (f) PU-2C-7B-1COOH at 200% strain.

7B-1COOH, and more change in conductivity is observed under the same strain.

4. CONCLUSIONS

To fabricate CPC strain sensors with tunable sensitivity, we used hybrid fillers of MWNTs and CB to modify the conductive network structure and additional MWNT-COOH was added to enhance the interfacial interaction between fillers and TPU. The effect of these two issues was investigated. In a comparison between CPCs containing only MWNTs (PU-10C) and hybrid fillers (PU-3C-7B), conductive network formed by hybrid fillers was observed to illustrate higher sensitivity of resistivity to strain. Furthermore, it was noted that the effect of using hybrid fillers and MWNT-COOH could be combined to enhance the sensitivity further as PU-2C-7B-1COOH demonstrated the highest sensitivity. These CPC samples were characterized to understand resistivity-strain relationship by SEM, Raman spectroscopy, WAXD, mechanical test, rheology-electrical measurement. It was concluded that less entangled network formed with hybrid fillers could give rise to higher sensitivity because the conductive network can be destructed more easily under strain. Furthermore, the use of additional MWNT-COOH leads to higher sensitivity by improving the interfacial interaction. Through the simple combination of these two issues, high-performance strain sensors could be fabricated with large strain-sensing capability (strain as large as 200%), and a wide range of tunable strain sensitivity (gauge factor ranges from 5 to 140238). These values are much larger than the results reported in literature for similar materials. Finally, an analytical model was used to analyze the results observed. It is observed that adjusting conductive network structure and interfacial interaction can accelerate the change of the number of conductive pathways and tunneling distance under strain. The change in these two issues is thought to be responsible for the strain-sensing behavior observed.

■ ASSOCIATED CONTENT

Ⓢ Supporting Information

This material includes 1 table of calculated parameters and 5 figures of the set-up for strain-sensing measurement, dynamic strain-sensing behavior, Raman shift, 2D-WAXD data and images, mechanical property and rheological property. The material is available free of charge via the Internet at http://pubs.acs.org.

■ AUTHOR INFORMATION

Corresponding Author

*Email: huadeng@scu.edu.cn (H.D.); qiangfu@scu.edu.cn (Q.F.). Tel: +86 28 8546 0953 (H.D.). Tel/Fax: +86 28 8546 1795 (Q.F.).

Notes

The authors declare no competing financial interest.

■ ACKNOWLEDGMENTS

We express our sincere thanks to the National Natural Science Foundation of China for financial support (51003063 and 51121001). This work was subsidized by the special funds for Major State Basic Research Projects of China (2011CB606006).

■ REFERENCES

(1) Zhao, Y. F.; Xiao, M.; Wang, S. J.; Ge, X. C.; Meng, Y. Z. *Composites Science and Technology* **2007**, *67*, 2528−2534.
(2) Dai, K.; Xu, X.-B.; Li, Z.-M. *Polymer* **2007**, *48*, 849−859.
(3) Pham, V. H.; Dang, T. T.; Hur, S. H.; Kim, E. J.; Chung, J. S. *ACS Appl. Mater. Interfaces* **2012**, *4*, 2630−2636.
(4) Aliev, A. E.; Oh, J.; Kozlov, M. E.; Kuznetsov, A. A.; Fang, S.; Fonseca, A. F.; Ovalle, R.; Lima, M. D.; Haque, M. H.; Gartstein, Y. N.; Zhang, M.; Zakhidov, A. A.; Baughman, R. H. *Science* **2009**, *323*, 1575−1578.
(5) Engel, J.; Chen, J.; Liu, C. *Appl. Phys. Lett.* **2006**, *89*, 221907−3.
(6) Gao, L. M.; Thostenson, E. T.; Zhang, Z.; Chou, T. W. *Adv. Funct. Mater.* **2009**, *19*, 123−130.
(7) O'Bryan, G.; Wong, B. M.; McElhanon, J. R. *ACS Appl. Mater. Interfaces* **2010**, *2*, 1594−1600.
(8) Zhang, X.; Pan, Y. *Polym. Int.* **2008**, *57*, 770−777.
(9) Hasan, T.; Sun, Z.; Wang, F.; Bonaccorso, F.; Tan, P. H.; Rozhin, A. G.; Ferrari, A. C. *Adv. Mater.* **2009**, *21*, 3874−3899.
(10) Lala, N.; Thavasi, V.; Ramakrishna, S. *Sensors* **2009**, *9*, 86−101.
(11) Olichwer, N.; Leib, E. W.; Halfar, A. H.; Petrov, A.; Vossmeyer, T. *ACS Appl. Mater. Interfaces* **2012**, *4*, 6151−6161.
(12) Hong, Y.; Su, M. *ACS Appl. Mater. Interfaces* **2012**, *4*, 3759−3764.
(13) Gao, S.-l.; Zhuang, R.-C.; Zhang, J.; Liu, J.-W.; Mäder, E. *Adv. Funct. Mater.* **2010**, *20*, 1885−1893.
(14) Enzo Pasquale, S.; Lorussi, F.; Mazzoldi, A.; De Rossi, D. *Sens. J., IEEE* **2003**, *3*, 460−467.
(15) Eswaraiah, V.; Balasubramaniam, K.; Ramaprabhu, S. *J. Mater. Chem.* **2011**, *21*, 12626−12628.
(16) Munro, B. J.; Campbell, T. E.; Wallace, G. G.; Steele, J. R. *Sens. Actuators, B* **2008**, *131*, 541−547.
(17) Yamada, T.; Hayamizu, Y.; Yamamoto, Y.; Yomogida, Y.; Izadi-Najafabadi, A.; Futaba, D. N.; Hata, K. *Nat. Nanotechnol.* **2011**, *6*, 296−301.
(18) Kollosche, M.; Stoyanov, H.; Laflamme, S.; Kofod, G. *J. Mater. Chem.* **2011**, *21*, 8292−8294.
(19) Schwalb, C. H.; Grimm, C.; Baranowski, M.; Sachser, R.; Porrati, F.; Reith, H.; Das, P.; Müller, J.; Völklein, F.; Kaya, A.; Huth, M. *Sensors* **2010**, *10*, 9847−9856.
(20) Hempel, M.; Nezich, D.; Kong, J.; Hofmann, M. *Nano Lett.* **2012**, *12*, 5714−5718.
(21) Murugaraj, P.; Mainwaring, D.; Khelil, N. A.; Peng, J. L.; Siegele, R.; Sawant, P. *Carbon* **2010**, *48*, 4230−4237.
(22) Dang, Z.-M.; Jiang, M.-J.; Xie, D.; Yao, S.-H.; Zhang, L.-Q.; Bai, J. *J. Appl. Phys.* **2008**, *104*, 024114−024114-6.
(23) Hwang, J.; Jang, J.; Hong, K.; Kim, K. N.; Han, J. H.; Shin, K.; Park, C. E. *Carbon* **2011**, *49*, 106−110.
(24) Lin, L.; Deng, H.; Gao, X.; Zhang, S.; Bilotti, E.; Peijs, T.; Fu, Q. *Polym. Int.* **2013**, *62*, 134−140.
(25) Mao, C.; Zhu, Y.; Jiang, W. *ACS Appl. Mater. Interfaces* **2012**, *4*, 5281−5286.
(26) Patole, A. S.; Patole, S. P.; Jung, S.-Y.; Yoo, J.-B.; An, J.-H.; Kim, T.-H. *Eur. Polym. J.* **2012**, *48*, 252−259.
(27) Ma, P.-C.; Liu, M.-Y.; Zhang, H.; Wang, S.-Q.; Wang, R.; Wang, K.; Wong, Y.-K.; Tang, B.-Z.; Hong, S.-H.; Paik, K.-W.; Kim, J.-K. *ACS Appl. Mater. Interfaces* **2009**, *1*, 1090−1096.
(28) Zhang, S.; Lin, L.; Deng, H.; Gao, X.; Bilotti, E.; Peijs, T.; Zhang, Q.; Fu, Q. *Colloid Polym. Sci.* **2012**, *290*, 1393−1401.
(29) Flandin, L.; Bréchet, Y.; Cavaillé, J. Y. *Compos. Sci. Technol.* **2001**, *61*, 895−901.
(30) Zhang, R.; Baxendale, M.; Peijs, T. *Phys. Rev. B* **2007**, *76*, 195433.
(31) Deng, H.; Skipa, T.; Bilotti, E.; Zhang, R.; Lellinger, D.; Mezzo, L.; Fu, Q.; Alig, I.; Peijs, T. *Adv. Funct. Mater.* **2010**, *20*, 1424−1432.
(32) Shang, S.; Zeng, W.; Tao, X.-m. *J. Mater. Chem.* **2011**, *21*, 7274−7280.
(33) Barick, A. K.; Tripathy, D. K. *Mater. Sci. Eng., B* **2011**, *176*, 1435−1447.
(34) Choudhury, A. *Mater. Chem. Phys.* **2011**, *130*, 231−236.

(35) Vukicevic, R.; Vukovic, I.; Stoyanov, H.; Korwitz, A.; Pospiech, D.; Kofod, G.; Loos, K.; Brinke, G. t.; Beuermann, S. *Polym. Chem.* **2012**, *3*, 2261−2265.
(36) Koerner, H.; Kelley, J. J.; Vaia, R. A. *Macromolecules* **2008**, *41*, 4709−4716.
(37) Loos, J.; Alexeev, A.; Grossiord, N.; Koning, C. E.; Regev, O. *Ultramicroscopy* **2005**, *104*, 160−167.
(38) Sekitani, T.; Noguchi, Y.; Hata, K.; Fukushima, T.; Aida, T.; Someya, T. *Science* **2008**, *321*, 1468−1472.
(39) Deng, H.; Skipa, T.; Zhang, R.; Lellinger, D.; Bilotti, E.; Alig, I.; Peijs, T. *Polymer* **2009**, *50*, 3747−3754.
(40) Bilotti, E.; Zhang, R.; Deng, H.; Baxendale, M.; Peijs, T. *J. Mater. Chem.* **2010**, *20*, 9449−9455.
(41) Chen, L.; Chen, G. H.; Lu, L. *Adv. Funct. Mater.* **2007**, *17*, 898−904.
(42) Knite, M.; Teteris, V.; Kiploka, A.; Kaupuzs, J. *Sens. Actuators A* **2004**, *110*, 142−149.
(43) Puglia, D.; Valentini, L.; Kenny, J. M. *J. Appl. Polym. Sci.* **2003**, *88*, 452−458.
(44) Hadjiev, V. G.; Iliev, M. N.; Arepalli, S.; Nikolaev, P.; Files, B. S. *Appl. Phys. Lett.* **2001**, *78*, 3193−3195.
(45) Valentini, L.; Biagiotti, J.; Kenny, J. M.; Santucci, S. *J. Appl. Polym. Sci.* **2003**, *87*, 708−713.
(46) Ma, P. C.; Kim, J.-K.; Tang, B. Z. *Compos. Sci. Technol.* **2007**, *67*, 2965−2972.
(47) Kim, Y. J.; Shin, T. S.; Choi, H. D.; Kwon, J. H.; Chung, Y.-C.; Yoon, H. G. *Carbon* **2005**, *43*, 23−30.
(48) Lima, A. M. F.; Castro, V. G. d.; Borges, R. S.; Silva, G. G. *Polímeros* **2012**, *22*, 117−124.
(49) Granero, A. J.; Wagner, P.; Wagner, K.; Razal, J. M.; Wallace, G. G.; Panhuis, M. I. H. *Adv. Funct. Mater.* **2011**, *21*, 955−962.
(50) Srivastava, R. K.; Vemuru, V. S. M.; Zeng, Y.; Vajtai, R.; Nagarajaiah, S.; Ajayan, P. M.; Srivastava, A. *Carbon* **2011**, *49*, 3928−3936.
(51) Vemuru, S. M.; Wahi, R.; Nagarajaiah, S.; Ajayan, P. M. *J. Strain Anal. Eng. Des.* **2009**, *44*, 555−562.
(52) Kang, I.; Schulz, M. J.; Kim, J. H.; Shanov, V.; Shi, D. *Smart Mater. Struct.* **2006**, *15*, 737−748.
(53) Cullinan, M. A.; Culpepper, M. L. *Phys. Rev. B* **2010**, *82*, No. 115428.
(54) Tong, J.; Sun, Y. *IEEE Trans. Nanotechnol.* **2007**, *6*, 519−523.
(55) Geim, A. K.; Novoselov, K. S. *Nat. Mater.* **2007**, *6*, 183−191.
(56) Fan, Q. Q.; Qin, Z. Y.; Gao, S. L.; Wu, Y. T.; Pionteck, J.; Mader, E.; Zhu, M. F. *Carbon* **2012**, *50*, 4085−4092.
(57) Robert, C.; Feller, J. F.; Castro, M. *ACS Appl. Mater. Interfaces* **2012**, *4*, 3508−3516.
(58) Slobodian, P.; Riha, P.; Saha, P. *Carbon* **2012**, *50*, 3446−3453.
(59) Ning, H.; Karube, Y.; Cheng, Y.; Masuda, Z.; Fukunaga, H. *Acta Mater.* **2008**, *56*, 2929−36.
(60) Zhang, R.; Deng, H.; Valenca, R.; Jin, J.; Fu, Q.; Bilotti, E.; Peijs, T. *Sens. Actuators, A* **2012**, *179*, 83−91.
(61) Hu, N.; Karube, Y.; Arai, M.; Watanabe, T.; Yan, C.; Li, Y.; Liu, Y.; Fukunaga, H. *Carbon* **2010**, *48*, 680−687.
(62) Walker, D. S.; Hellinga, H. W.; Saavedra, S. S.; Reichert, W. M. *J. Phys. Chem.* **1993**, *97*, 10217−10222.
(63) Deng, H.; Bilotti, E.; Zhang, R.; Peijs, T. *J. Appl. Polym. Sci.* **2010**, *118*, 30−41.
(64) Liang, D.; Zhou, L.-j.; Zhang, Q.; Chen, F.; Wang, K.; Deng, H.; Fu, Q. *Chin. J. Polym. Sci.* **2012**, *30*, 603−612.
(65) Jiang, K.; Yu, F. L.; Su, R.; Yang, J. H.; Zhou, T. N.; Gao, J.; Deng, H.; Wang, K.; Zhang, Q.; Chen, F.; Fu, Q. *Chin. J. Polym. Sci.* **2011**, *29*, 456−64.
(66) Koerner, H.; Liu, W. D.; Alexander, M.; Mirau, P.; Dowty, H.; Vaia, R. A. *Polymer* **2005**, *46*, 4405−4420.
(67) Wang, Z.; Ciselli, P.; Peijs, T. *Nanotechnology* **2007**, *18*, 455709.
(68) Potschke, P.; Abdel-Goad, M.; Alig, I.; Dudkin, S.; Lellinger, D. *Polymer* **2004**, *45*, 8863−8870.
(69) Aranguren, M. I.; Mora, E.; DeGroot, J. V., Jr.; Macosko, C. W. *J. Rheol.* **1992**, *36*, 1165−82.
(70) Zhang, X.-W.; Pan, Y.; Zheng, Q.; Yi, X.-S. *J. Polym. Sci., Part B* **2000**, *38*, 2739−2749.
(71) Simmons, J. G. *J. Appl. Phys.* **1963**, *34*, 1793−1803.
(72) Sheng, P.; Sichel, E. K.; Gittleman, J. I. *Phys. Rev. Lett.* **1978**, *40*, 1197−1200.
(73) Mrozek, R. A.; Cole, P. J.; Mondy, L. A.; Rao, R. R.; Bieg, L. F.; Lenhart, J. L. *Polymer* **2010**, *51*, 2954−2958.